

$^{12}\text{C} + ^{16}\text{O}$ Elastic Scattering and Total Reaction Cross Sections near the Coulomb Barrier

B. N. Nagorecka,^{A,B} G. D. Symons,^A P. B. Treacy^A and I. C. Maclean^A

^A Department of Nuclear Physics, Research School of Physical Sciences, Australian National University, P.O. Box 4, Canberra, A.C.T. 2600.

^B Present address: Division of Computing Research, CSIRO, P.O. Box 1800, Canberra City, A.C.T. 2601.

Abstract

Elastic scattering and total reaction cross sections (via γ ray yields) have been measured for $^{16}\text{O} + ^{12}\text{C}$ in the c.m. energy range 5.5-10.0 MeV. Some well-defined structure is observed, with peak widths of order 250 keV. An optical potential which fits peaks in the total reaction cross section is shown to be inadequate to explain the elastic scattering data. Possible reasons for this inconsistency, which imply the need for a more general optical potential, are discussed.

1. Introduction

It has been observed that pronounced resonance structure exists in reaction cross sections for entrance channels for $^{12}\text{C} + ^{12}\text{C}$ (Almqvist *et al.* 1960; Patterson *et al.* 1969; Mazarakis and Stephens 1972) and $^{12}\text{C} + ^{16}\text{O}$ (Patterson *et al.* 1971) in the region of the Coulomb barrier energy. Similar, but far less prominent, structure of somewhat greater width has been observed (Spinka and Winkler 1972) in $^{16}\text{O} + ^{16}\text{O}$. A recent attempt (Nagorecka and Newton 1972) to describe the $^{12}\text{C} + ^{16}\text{O}$ reaction data in terms of single-particle states of the entrance channel, using an optical potential, resulted in a reasonably good fit to the peak positions. If this approach is valid, these peaks should appear in elastic scattering. That this is so can be seen for the special case of zero-spin channels c and c' with orbital angular momenta l and l' . The reaction amplitude for transitions $c \rightarrow c'$ may be written (Lane and Thomas 1958) as

$$A_{c'c}(\theta') = \frac{\pi^{1/2}}{k_c} \left\{ -C_{c'}(\theta_{c'}) \delta_{c'c} + \sum_{l'} (2l+1)^{1/2} T_{l'l} \left(\frac{2l'+1}{4\pi} \right)^{1/2} P_{l'}(\cos \theta_{c'}) \right\}, \quad (1)$$

where $C_{c'}(\theta_{c'})$ is a Coulomb amplitude for c.m. angle θ' , and $T_{l'l}$ is the element of the matrix $\exp(2i\omega) - U$. For an isolated resonance we may write

$$U_{l'l} = l^{i(\omega_{l'} + \omega_l - \phi_{l'} - \phi_l)} (\delta_{l'l} + i\Gamma_l^{1/2} \Gamma_{l'}^{1/2} / D), \quad (2)$$

where the ω_i and ϕ_i are Coulomb and background phase shifts respectively, the Γ_i are partial widths, and D is a resonance denominator. In the optical model, use is made of the quantity (for $l = l'$)

$$\eta_l = \exp(2i\omega_l) U_{ll}. \quad (3)$$

Equation (2) shows that if $A_{c'c}$ (for $c' \neq c$) contains resonances via $\Gamma_l^{1/2} \Gamma_{l'}^{1/2}$ then A_{cc} will depend on the Γ_l directly (albeit diluted by the nonzero Coulomb amplitude).

Equation (1) also shows that a given incident $l = l'$ leads to a well-defined angular dependence through the Legendre polynomial $P_l(\cos \theta_c)$. It was therefore proposed to measure scattering at angles chosen to highlight (maximize or minimize) chosen low l values. This is, of course, a well-known technique in elastic scattering studies.

In addition to observing elastic scattering, it was also decided to remeasure the total $^{12}\text{C} + ^{16}\text{O}$ cross section. Earlier work (Patterson *et al.* 1971) was done with relatively thick ($\sim 45\text{--}90$ keV) carbon targets, and in addition low energy reaction products were not recorded. We chose to use the method of recording final-state de-excitation γ rays, using a thin target with close detector geometry to compensate for low yields. This method, though sensitive only to reactions to excited states, does not bias against low energy products and gives a good measure of the total reaction cross section.

The total cross section measurements are reported in Section 2, and the elastic scattering observations in Section 3. In Section 4, details of optical potential fits to reaction and scattering data are described, and the results are discussed in Section 5.

2. Total $^{12}\text{C} + ^{16}\text{O}$ Reaction Cross Section from γ Ray Yields

(a) Experimental Procedure

A beam of ^{16}O ions (~ 50 particle nanoamperes) was accelerated by the ANU model EN tandem accelerator and collimated by two 2.3 mm diameter apertures 15 cm apart, 60 cm from the target position. A thin self-supporting natural carbon target of $5 \mu\text{g cm}^{-2}$ surface density was employed, except for the lowest energies at which it was necessary to use a thicker ($40 \mu\text{g cm}^{-2}$) foil. The beam intensity and thickness were monitored by a $100 \mu\text{m}$ thick silicon surface-barrier detector set at an angle of 60° . De-excitation γ rays were detected with a 7.6×7.6 cm (diameter \times length) NaI(Tl) scintillation counter set at 90° to the beam direction, with its face 3 cm from the target. Using this arrangement, it was possible to measure the γ ray yield while correcting for target thickness increase (due to carbon build-up) by detecting only ^{12}C recoils with the monitor detector.

All γ ray spectra were recorded for energies above 900 keV. Detection of lower energies was precluded by the presence of radiations from ^{56}Co induced in the beam lines; this, unfortunately, prevented detection of radiation from known levels (Endt and Van der Leun 1967) in ^{27}Si and ^{27}Al at 780 and 843 keV respectively. However, many of the higher low-lying excited states of these nuclei decay mainly direct to their ground states.

Certain experimental precautions were necessary during the taking of data owing to the great variation of yields (four orders of magnitude over the range covered). It was necessary to allow for background in the γ ray counter. This was due partly to the presence of ^{40}K in the laboratory walls and partly to ^{56}Co permanent radioactivity in the beam line and scattering chamber. It was reduced by shielding the detector with lead, but was allowed for in all cases.

Basically, the proportionality of the de-excitation γ ray yield to the total integrated cross section is only approximate, and essentially only justified when very many γ rays are simultaneously detected. In the present case, the yield was compared with actually measured cross sections (Patterson *et al.* 1971) over the energy range $5.4\text{--}10.0$ MeV. Satisfactory agreement (to within 10% between the relative yields) was obtained.

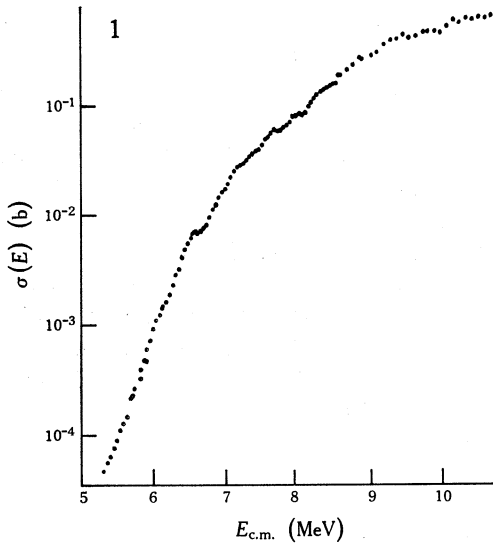
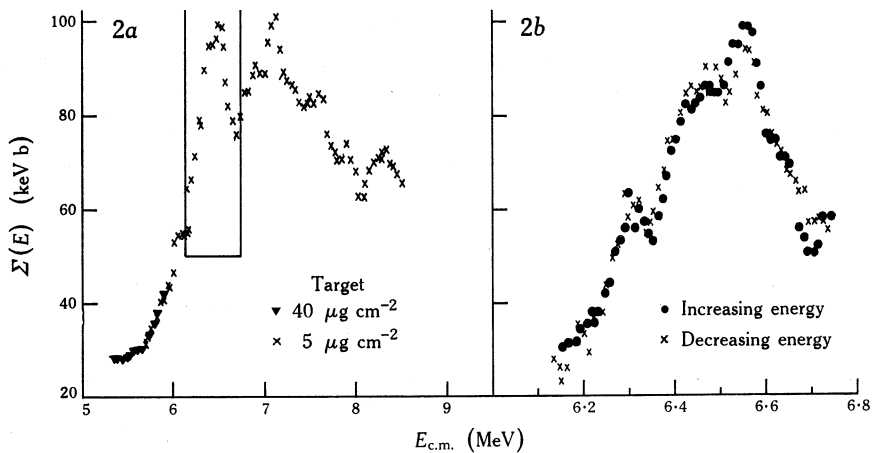


Fig. 1. Absolute cross section $\sigma(E)$ for the $^{12}\text{C}+^{16}\text{O}$ reaction obtained from measurements of the γ ray yield (see text).

Fig. 2. Excitation function of the Σ factors derived from the total γ ray yield from the $^{12}\text{C}+^{16}\text{O}$ reaction. The inset in (a) is reproduced in (b) to higher resolution. Small-amplitude fluctuations are seen superimposed on the broad and very prominent resonance at 6.5 MeV.



(b) Results

Gamma ray measurements were made at intervals of 43 keV over the range 5.4–10.5 MeV (where all energies are understood to be measured in the c.m. system unless otherwise indicated). The data are shown in Fig. 1. The absolute cross section scale was obtained from the average figures of Patterson *et al.* (1971), with an estimated correction factor of 1.1 to allow for a neutron yield unobserved in that work. Fig. 2a shows the factor $\Sigma(E)$ defined by the reduction of the cross section $\sigma(E)$ to the form (Patterson *et al.* 1971)

$$\sigma(E) = \{\Sigma(E)/E\} \sum_l (2l+1) \mathcal{P}_l \quad (4)$$

summed over incident orbital angular momenta l , with R matrix Coulomb penetration factors \mathcal{P}_l for a channel radius of 6.73 fm. Statistical errors in Fig. 2a are of order 1%, but systematic variations due to target-thickness effects and other experimental causes amount to 3%. The energy resolution is good (about 15 keV) and permits

identification of resonance peaks at 6.9, 7.1, 7.6 and 7.9 MeV, in addition to those already seen (Patterson *et al.* 1971) at 6.1, 6.5 and 8.3 MeV.

In Fig. 2a there appear to be several small peaks superimposed on the broad peak occurring at 6.5 MeV. To investigate these further, more detailed measurements were made in the energy range 6.15–6.75 MeV (see Fig. 2b). Here the circles (crosses) represent data taken in rising (falling) sequence with energy intervals of 10 keV, and it is clear that the correction of the effective bombarding energy for target thickness effects has been made correctly. Peaks in the data of Fig. 2b appear clearly at 6.31, 6.45 and 6.55 MeV, all with widths about 60 keV. One might consider that such peaks were genuine resonances, considering that a measured correlation width in this reaction has been estimated (Halbert *et al.* 1967) as 125 keV at 31 MeV. However, the correlation width at the present energy of around 6.5 MeV would certainly be smaller, and we consider that the small peaks might well be attributed to fluctuations. The question of the possible interpretation of the other peaks reported here is considered in the next section.

3. Differential Elastic-scattering Excitation Functions

(a) Experimental Details: Angular Accuracy

A beam of ^{16}O ions was used in the range 12–24 MeV (lab.) and collimated through two 1.5 mm diameter collimators, each followed by a 2.3 mm diameter antiscatter baffle, onto a self-supporting $5\ \mu\text{g cm}^{-2}$ natural carbon target mounted in a 44 cm diameter scattering chamber. Four 120 μm thick silicon surface-barrier detectors, collimated by 5×1 mm (vertical \times horizontal) slits mounted 18.2 cm from the target, were used to detect the scattered and recoiling ions.

Table 1. Angle setting of detectors for elastic scattering

Directions of local zeros of Legendre polynomials are given in square brackets

Detector angle (lab.)	Low energy ^{16}O angle (c.m.)	High energy ^{16}O angle (c.m.)	^{12}C angle (c.m.)
45.0°	$154.5 \pm 0.2^\circ$ [154.02° ($l = 5$)]	$115.6 \pm 0.7^\circ$ [109.9° ($l = 4$)]	$90.0 \pm 0.4^\circ$ [90.0° ($l = 1,3,5,\dots$)]
47.15°	$149.5 \pm 0.3^\circ$ [149.4° ($l = 4$)]	$124.9 \pm 0.9^\circ$ [125.3° ($l = 2$)] [122.6° ($l = 5$)]	$85.7 \pm 0.4^\circ$

Knowing alone the masses of ^{16}O and ^{12}C , it can be shown that kinematically the ^{16}O can not be emitted at angles backward of 48.61° (lab.). By rotating detectors on both sides of the beam, this fact was used to provide a calibration of detector angles to an accuracy within 0.05° (lab.) at the subtended detector angles of $\pm 0.3^\circ$ (c.m.). However, the effective beam spot size of ~ 2.5 mm increased the latter figure to $\pm 0.4^\circ$ at 90° (c.m. for ^{16}O).

Angles of two of the four detectors were chosen to be at zeros of certain Legendre polynomials, in accordance with the procedure outlined in Section 1. The angle settings are listed in Table 1, together with the effective c.m. angles for ^{16}O and ^{12}C , and actual or nearby polynomial zeros. The other two detectors were used as monitors set at 60° (lab.) on opposite sides of the beam. At this angle the ^{12}C recoils could be assumed to result with high accuracy from pure Coulomb scattering.

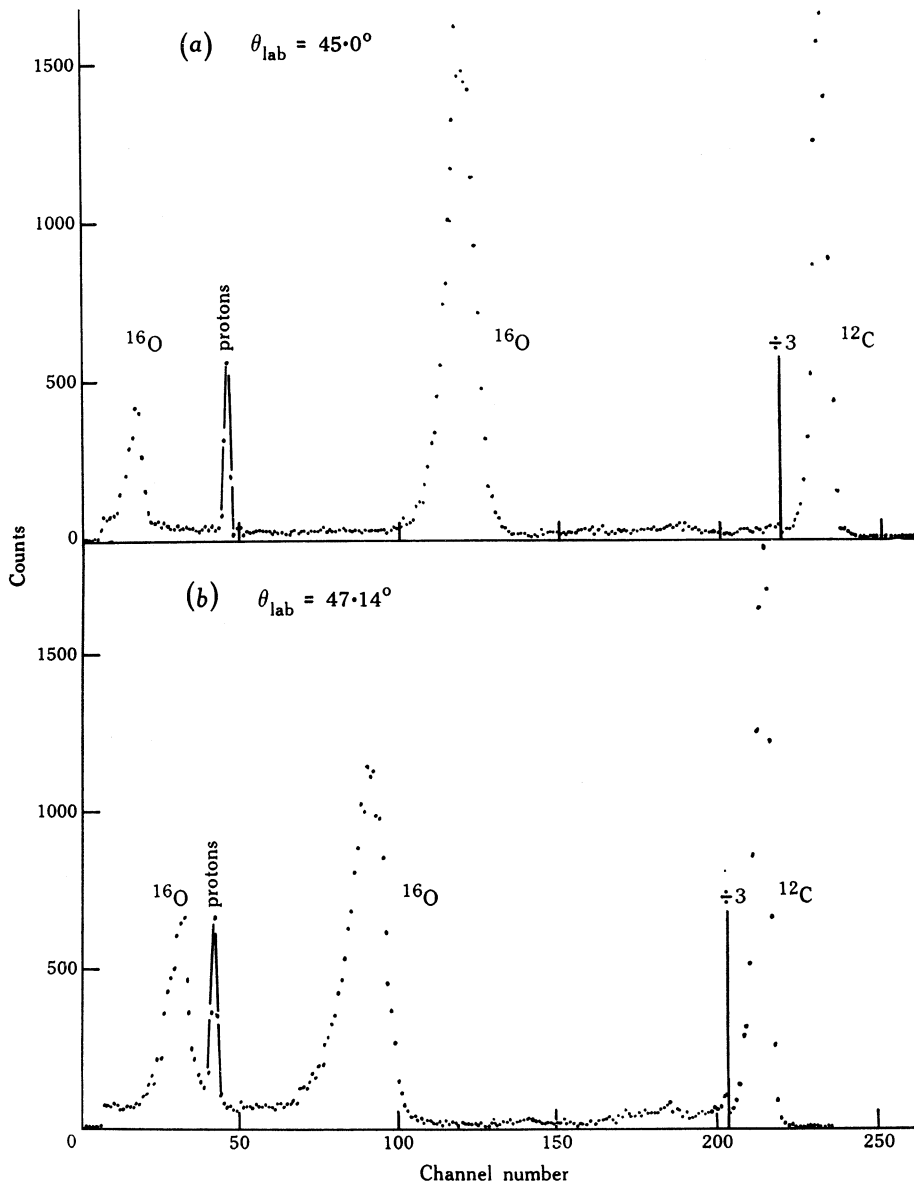
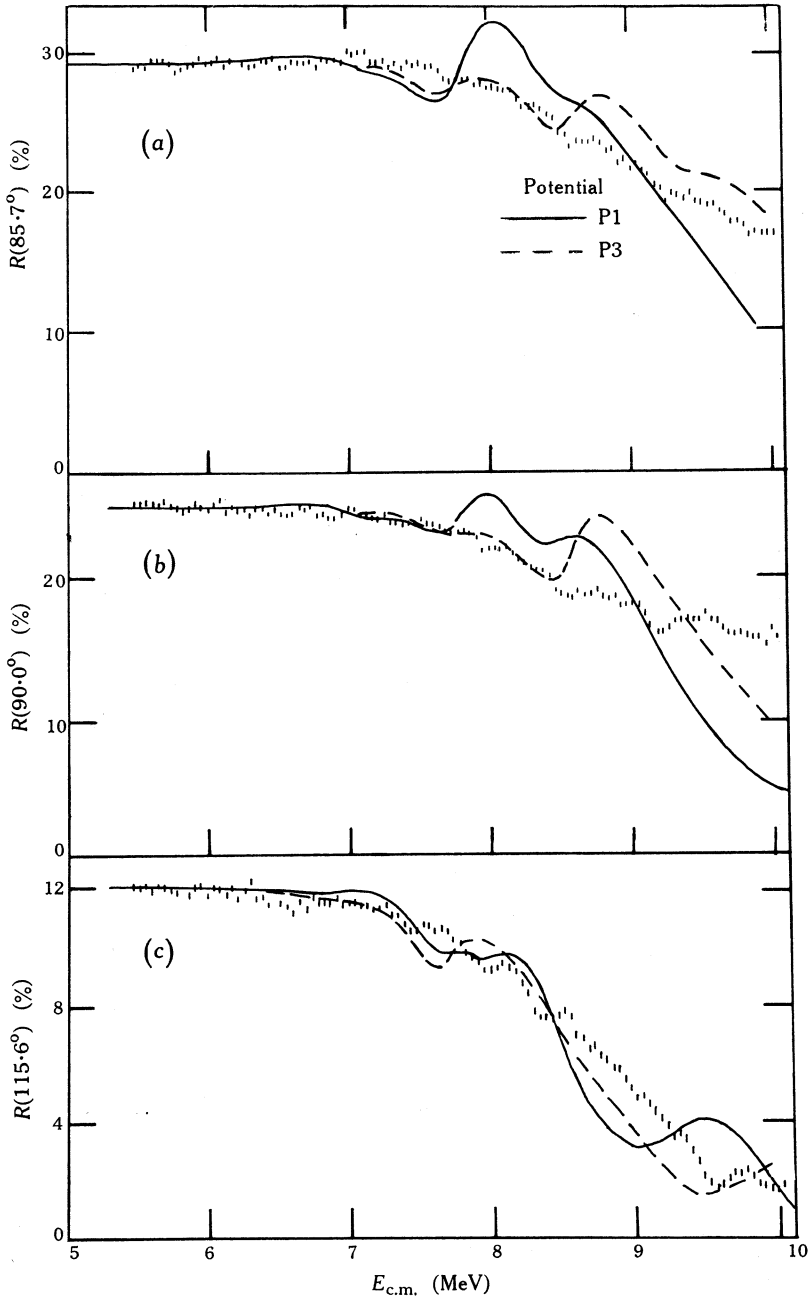


Fig. 3. Examples of particle spectra at laboratory angles of (a) 45.0° (counter 2) and (b) 47.14° (counter 3), for $E_{\text{lab}} = 18.6$ MeV. Two scattered ^{16}O peaks and a ^{12}C recoil peak can be seen, the effective c.m. angles for which are given in Table 1. The proton recoil group due to impurities in the target is also evident.

(b) Results

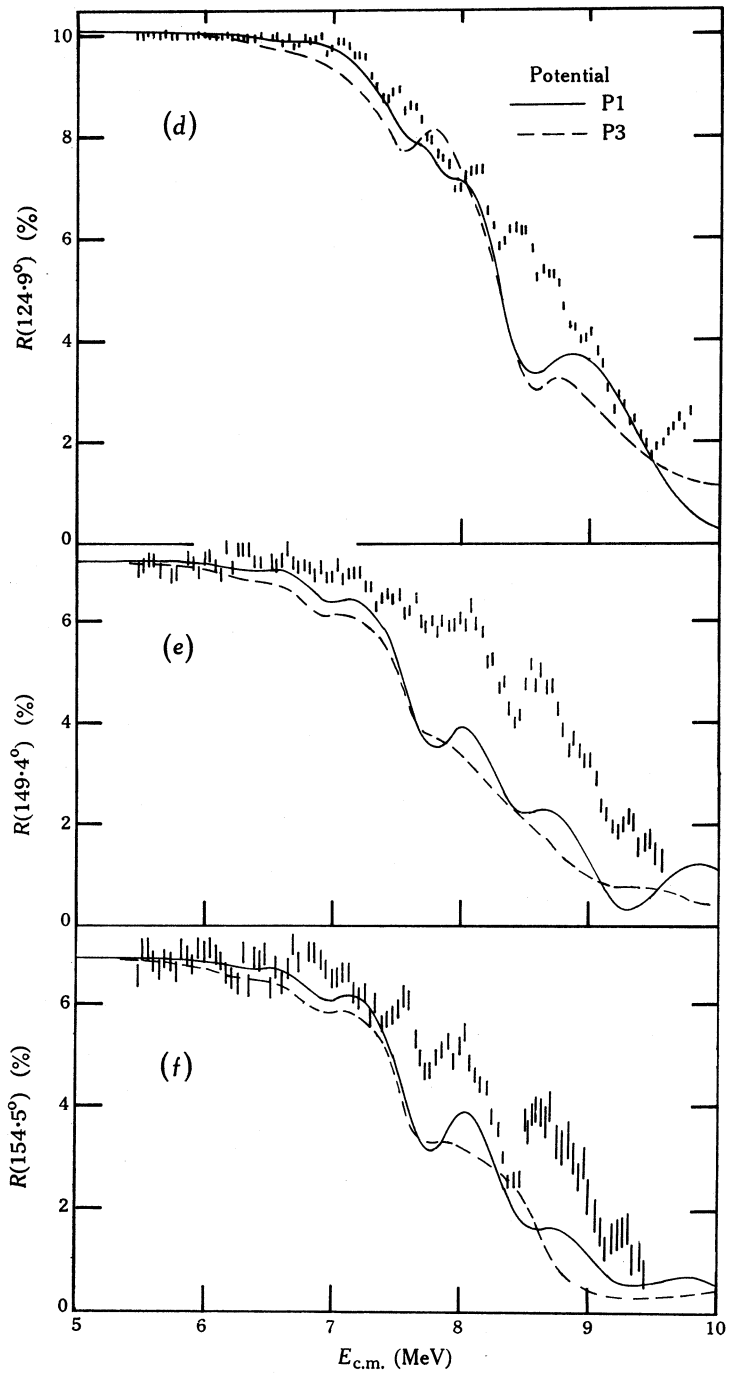
Typical particle spectra, taken at the laboratory angles of 45.0° and 47.14° , are shown in Fig. 3. In addition to the three groups indicated in Table 1, there is a sharp group (near channel 40) attributable to recoil protons from hydrogen in the target. It is clear that the two lower energy peaks due to ^{16}O ions require careful analysis for their summation into areas. The 'tails' must be attributed in part to incident



Figs 4a-4f. Excitation functions of the ratio

$$R(\theta) = \frac{d\sigma(\theta)/d\Omega}{d\sigma(60^\circ)/d\Omega},$$

where the numerator and denominator are $^{12}\text{C} + ^{16}\text{O}$ differential elastic scattering cross sections. Results are for centre of mass angles of (a) 85.7° , (b) 90.0° , (c) 115.6° , (d) 124.9° , (e) 149.5° , (f) 154.5° . Experimental data are those of Section 3b, and theoretical curves are predictions of the optical model using the indicated potentials.



Figs 4d-4f

beam inhomogeneity, but also to detector degradation. In the analysis an attempt was made to measure the same *fraction* of all peak areas, and the results were calculated as ratios to ^{12}C (Coulomb) scattering at 60° (lab.). Then the calculated fractions were renormalized by assuming that the calculated ratios must become equal to known constants at low energies.

Table 2. Parameters of optical potentials

Parameter (Eqns 5,6)	Parameter value in potential model			
	P1	P2	P3	P4
V (MeV)	-8.1	-8.1	-10.5	-10.5
R_r/R_0	1.37	1.37	1.22	1.22
a_r (fm)	0.6	0.6	0.9	0.9
U_{REP} (MeV)	0.0	0.0	50.0	50.0
R_u (fm)	—	—	3.5	3.5
W (MeV)	-1.8	$W(E)^*$	-1.8	$W(E)^*$
R_i/R_0	1.35	1.35	1.35	1.35
a_i (fm)	0.5	0.5	0.5	0.5
R_c/R_0	1.4	1.4	1.2	1.2
C (MeV)	0.0008	0.0	0.0008	0.0
k	0.0	0.0	-0.15	-0.15

* For models P2 and P4 we have

$$\begin{aligned}
 W &= -0.54E + 1.45 \quad \text{for } 4.5 \leq E \leq 10.0 \text{ MeV,} \\
 &= -3.95E \quad \quad \quad 10.0 \text{ MeV} < E.
 \end{aligned}$$

Spectra were recorded at energy intervals of 43 keV between 5.4 and 10.0 MeV. Their energy scales were established using the known proton and ^{12}C recoil peaks. The results, shown in Figs 4a-4f, display some obvious resonance structure, namely at 7.1, 7.6 and 8.3 MeV, which is strongest at the most backward angles (c.m. angles 154.6° and 149.4°). Generally, the resonances appear as weak interference peaks superimposed on the predominantly smooth Coulomb yield, and the results are rather disappointing for delineating structure, when compared with those of Fig. 2. This was, of course, to be expected, because of the presence of Coulomb scattering. The resonances mentioned are, however, certainly statistically significant.

In outline, the results of Sections 2 and 3 appear to show the existence of eight resonances in the region studied. Those of Section 2 (Fig. 2) are prominent well beyond the predicted figure of $\lesssim 3\%$ estimated (Nagorcka 1973) for statistical fluctuations, based on only the number of α particle channels. The justification for the resonances discussed in the present section (Fig. 4) rests on the fact that each of the three peaks is seen to occur at at least two different angles.

4. Fits to Data using Woods-Saxon Optical Potentials

Recent attempts to apply the conventional optical model to heavy ion reactions have achieved some degree of success in fitting elastic scattering data. Previous attempts to fit the $^{12}\text{C}+^{16}\text{O}$ (Kuehner and Almqvist 1964) and $^{12}\text{C}+^{12}\text{C}$ (Michaud and Vogt 1972) total reaction cross section data using the optical model have assumed that the resonances occurring in the total reaction cross section should be averaged and the fit applied to the average. This would indeed be the case if the resonances

were the doorway states suggested by Michaud and Vogt (1972). However, the strong correlation existing in the total α and total p cross sections for both the $^{12}\text{C} + ^{16}\text{O}$ and $^{12}\text{C} + ^{12}\text{C}$ reactions, together with the apparent lack of resonances below 6 MeV in the former reaction, led us to search for a potential which would reproduce the resonances in the form of single-particle resonances in a complex optical potential.

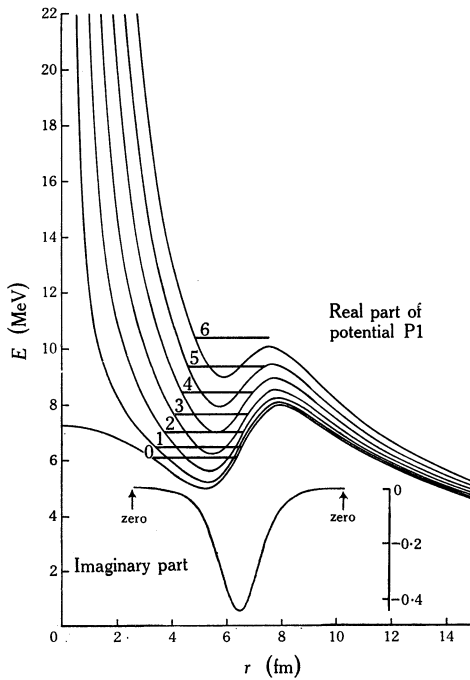


Fig. 5. Real (for $l = 0$ to 6) and imaginary parts of the optical model potential P1. Horizontal lines indicate the 'energy level' where the nuclear phase shift resonates for the indicated l values. For $C = 0.0008$ MeV (which cannot be distinguished from $C = 0$ on this scale), the imaginary part vanishes identically for $R < 2.6$ and $R > 10.3$ fm.

Calculations using four optical potentials are discussed in this section. These potentials are defined by

$$V_l(r) = V_n(r) + \frac{2}{3}(Z_1 Z_2 e^2/R_c)F + \hbar^2 l(l+1)/2mr^2, \quad (5)$$

where

$$\left. \begin{aligned} F &= 1 - \frac{1}{3}(r/R_c)^2 & \text{for } r < R_c \\ &= \frac{2}{3}R_c/r & \text{for } r \geq R_c, \end{aligned} \right\} \quad (6a)$$

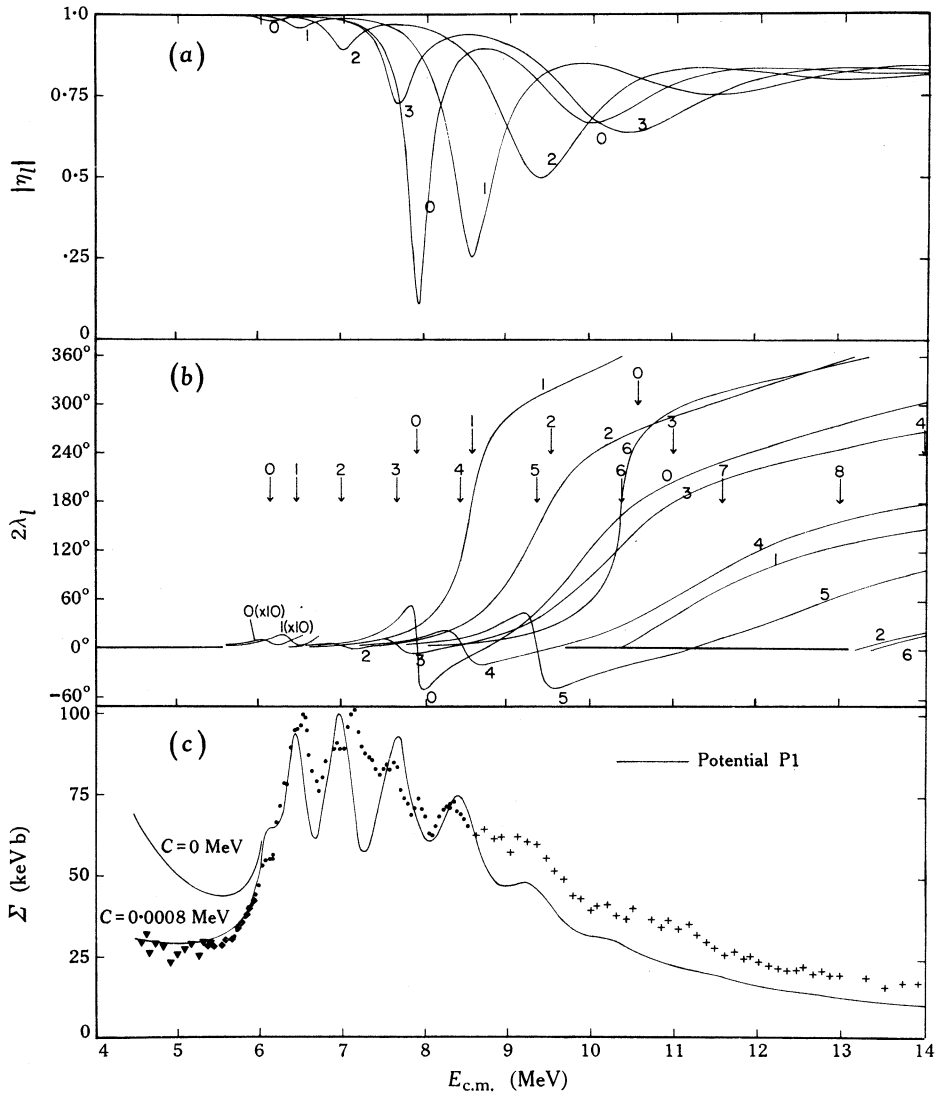
and

$$V_n(r) = \frac{V}{1 + \exp((r - R_r)/a_r)} + U_{\text{REP}} + \frac{iW \exp((r - R_i)/a_i)}{\{\exp((r - R_i)/a_i)\}^2} + iC, \quad (6b)$$

with

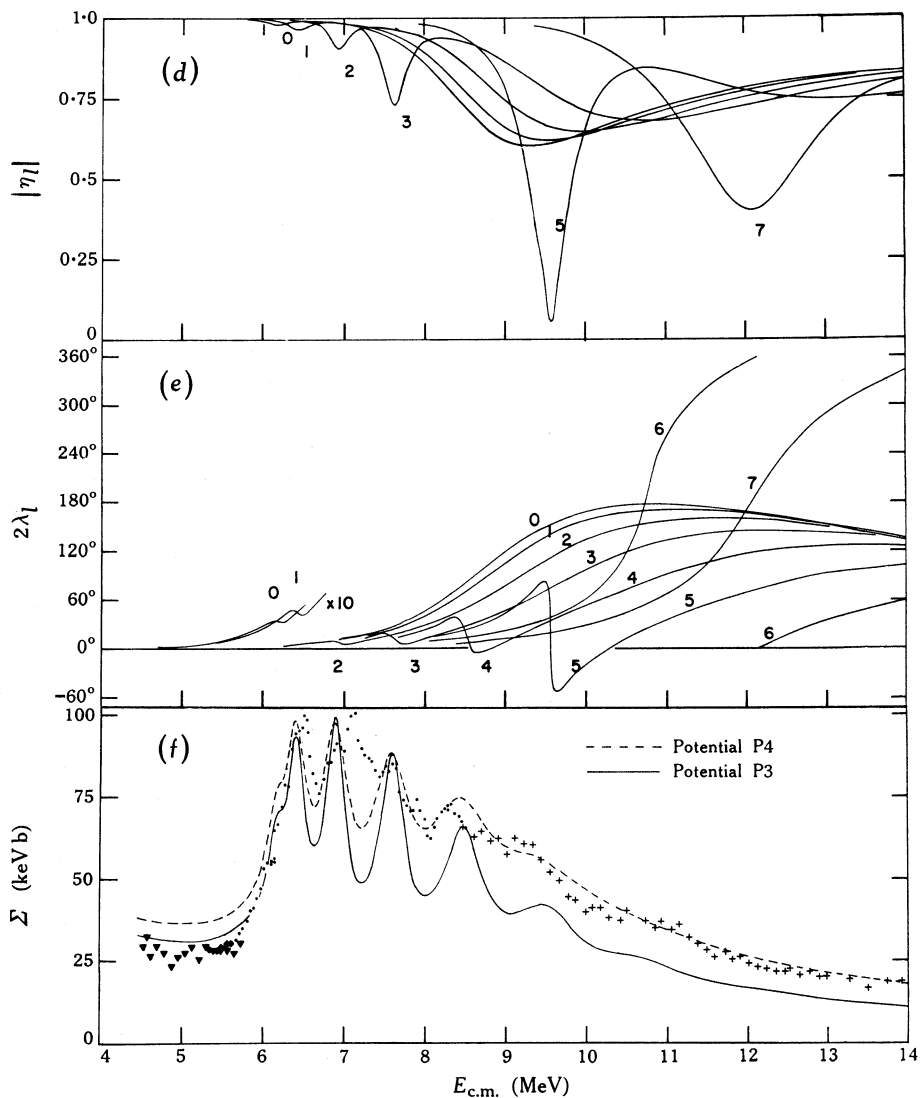
$$\left. \begin{aligned} U_{\text{REP}} &= U_R & \text{for } r < R_u \\ &= 0 & \text{for } r \geq R_u. \end{aligned} \right\} \quad (6c)$$

The four potentials are denoted P1, P2, P3 and P4. The values of the parameters which determine them are listed in Table 2. All potentials have shallow attractive parts, consistent with the results of some theoretical calculations (Mosel *et al.* 1970; Pruess and Greiner 1970; Reidmeister 1972).



Figs 6a-6c. Plot as a function of energy of (a) the magnitude of the reflection coefficient η_l and (b) the nuclear phase shift λ_l for the indicated l values. The curves were calculated using potential P1, and were used to determine the total reaction cross section and hence the Σ factor (solid curve) shown in (c). The results in (c) are for the ratio of the differential elastic scattering cross section at 154.5° to that at 60° (c.m.). The experimental data are:

- triangles, charged particle yields from Patterson *et al.* (1969);
- diamonds, integrated γ ray yields using $40 \mu\text{g}$ target;
- circles, integrated γ ray yields using $5 \mu\text{g}$ target;
- pluses, total $^{12}\text{C}+^{16}\text{O}$ cross section measurements from Kuehner and Almqvist (1964).



Figs 6d-6f. Plot as a function of energy of (d) the magnitude of the reflection coefficient η_l and (e) the nuclear phase shift λ_l , for the indicated l values. The curves were calculated using potentials P3 and P4, and were used to determine the total reaction cross sections and hence the Σ factors (solid and dashed curves as indicated) in (f). The experimental data are the same as in Fig. 6c.

(a) $^{12}\text{C} + ^{16}\text{O}$ Total Reaction Cross Section

Potential P1 is shown in Fig. 5 together with the energies at which resonances corresponding to various l values, in equations (1)–(3), occur in this potential. Potential P1 was obtained by fitting the Σ factors in Fig. 6c, and interpreting the structure seen in the reaction data as resonances of an optical potential. As can be seen from Fig. 6b, this approach proved reasonably successful.

Redefining η_l of equation (1c) as

$$\eta_l = \exp(2i\delta_l)$$

and further defining

$$\lambda_l = \text{Re}(\delta_l),$$

we then plot λ_l in Fig. 6b and $|\eta_l|$ in Fig. 6a for the potential P1. The degree of absorption occurring in P1 due to $V_n(R)$ is therefore indicated in Fig. 6a, while the lower, middle and upper sets of arrows in Fig. 6b indicate the energies where the system resonates for a given l value for the first, second and third time respectively. These calculations are discussed in more detail by Nagorcka and Newton (1972).

Much has been written about the use of the optical model in describing heavy ion reactions such as $^{12}\text{C} + ^{12}\text{C}$, $^{12}\text{C} + ^{16}\text{O}$ and $^{16}\text{O} + ^{16}\text{O}$, and whether or not a repulsive core should be included in the optical potential (Brueckner *et al.* 1968; Scheid and Greiner 1969; Mosel *et al.* 1970; Pruess and Greiner 1970; Fliessbach 1971; Reidmeister 1972). Therefore we have attempted to fit the $^{12}\text{C} + ^{16}\text{O}$ total reaction using potential P3. To obtain P3, a square repulsive core 50 MeV high was added to P1. This produced relatively small changes in the total reaction cross section, provided the width of the core was less than 1.5 fm. When the width was increased beyond 1.5 fm, the $l = 0$ shoulder at 6.1 MeV became much less prominent.

The width of this core was made 3.5 fm, and attempts were made to adjust the remaining parameters to compensate for the effect of the repulsive core. This was possible if the second term of equation (5) was changed, with some physical justification (Nagorcka 1973), to

$$\begin{aligned} \{1 - k(r - R_c)\}^{\frac{3}{2}} (Z_1 Z_2 e^2 / R_c) \{1 - \frac{1}{3}(r/R_c)^2\} & \quad \text{for } r < R_c, \\ Z_1 Z_2 e^2 / r & \quad r \geq R_c. \end{aligned}$$

This defines potential P3 if we have $k = -0.15$ (Table 2). Other parameters are given in Table 2 and the potential itself is shown in Fig. 7.

The square repulsive core has the effect of raising the energy of each resonance—an effect which decreases as the l value associated with the resonance increases. This occurs because the centrifugal potential is itself a repulsive core (see Fig. 5) which increases in width and magnitude as the l value increases. The square repulsive core therefore decreases the spacing of the resonances. Since these resonances are due to successive l values, it is possible to increase the spacing again by:

- (1) Including the factor $\{1 - k(r - R_c)\}$ for $r < R_c$ as stated above, thus making P3 deeper at smaller values of the separation distance r (see Fig. 7).
- (2) Decreasing R_r to 1.22. However, this lowers the absolute cross section which must be compensated for by increasing a_r .

The results of calculations for potential P3 are shown in Figs 6d–6f. The calculated Σ factors (continuous curve) are compared with experimental values in Fig. 6f, while

the magnitude of η_l and the phase shifts are shown in Figs 6*d* and 6*e* respectively for l values 0–7.

The fits obtained using potentials P1 and P3 are quite comparable. However, there is one major difference: the addition of a repulsive core has removed all resonances corresponding to the middle and upper sets of arrows in Fig. 6*b*. This result may be important in providing a way to determine whether or not a repulsive core exists for data with some well-established and fitted resonances. Finally, it should be noted that the fits to the Σ factors in Figs 6*c* and 6*f* can be improved by changing the imaginary parts of potentials P1 and P3 to one which increases with energy. The new potentials, P2 and P4, are defined in Table 2. An example of the improved fit can be seen in Fig. 6*f* (dashed curve).

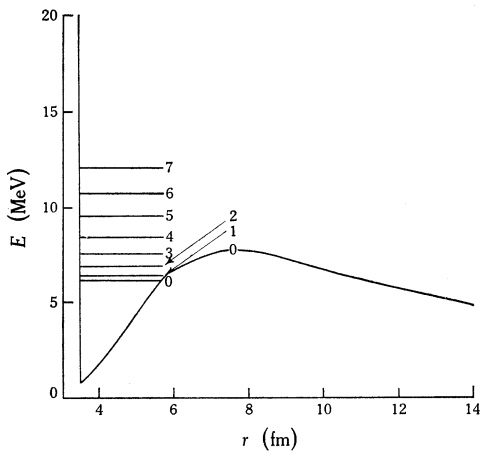


Fig. 7. Real part of potential P3 (and P4), showing the square repulsive core 3.5 fm wide and the energies (horizontal lines) at which the indicated l values resonate. The imaginary part of P3 is the same as that for P1 shown in Fig. 5.

(b) $^{12}\text{C}(^{16}\text{O}, \alpha_0)^{24}\text{Mg}$ Angular Distributions

The attempts to fit the total reaction cross section using the optical model, discussed in the previous subsection, were based on the assumption that resonances seen at 6.1, 6.5, 7.1, 7.6 and 8.3 MeV are due predominantly to spins 0, 1, 2, 3 and 4 respectively. It may be possible to test this assumption by considering the angular distributions of the $^{12}\text{C}(^{16}\text{O}, \alpha_0)^{24}\text{Mg}$ reaction. It should be noted that Groce and Lawrence (1965) listed resonances in the integrated $^{12}\text{C}(^{16}\text{O}, \alpha_0)^{24}\text{Mg}$ reaction at 7.1, 7.7 and 8.6 MeV plus a 'prominent shoulder' at 6.7, 8.3 and 8.8 MeV.

Angular distributions for $^{12}\text{C}(^{16}\text{O}, \alpha_0)^{24}\text{Mg}$ have been measured by Groce and Lawrence (1965) in energy intervals of 145 keV. We have attempted to minimize the effects of statistical fluctuations in these results by averaging them over energy ranges of the order of 300 keV (c.m.) where resonances are expected (Nagorcka 1973). This was done by first weighting each angular distribution by the reciprocal of the Coulomb penetration factors for the incoming channel (that is, \mathcal{P}_l in equation 4) and then summing several angular distributions together over the energy regions where particular spins were assumed to dominate. The results were compared with α_0 angular distributions predicted by Hauser-Feshbach calculations, using transmission coefficients for the $^{12}\text{C}+^{16}\text{O}$ channel calculated with potential P3. Transmission coefficients for p, n, d and α outgoing channels were calculated using potentials from Rosen *et al.* (1965), Rosen *et al.* (1965), Perey and Perey (1963), and McFadden and Satchler (1966) respectively. These calculations are reported in more detail by

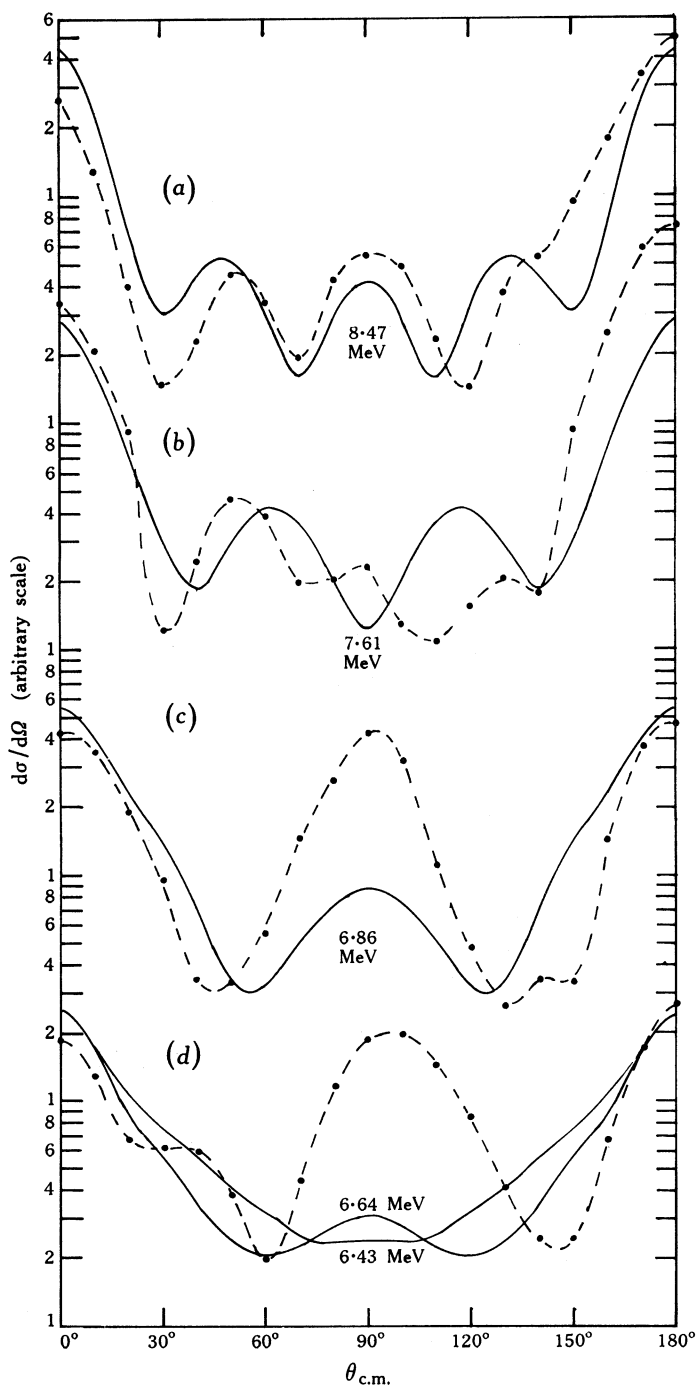


Fig. 8. Comparison of averaged $^{12}\text{C}(^{16}\text{O}, \alpha)^{24}\text{Mg}$ angular distributions from the data of Groce and Lawrence (1965) (dashed curves) with the Hauser-Feshbach predictions (solid curves) calculated using potential P3 for the indicated c.m. energies.

Nagorcka (1973). The results are shown in Fig. 8, together with the energies at which the calculations were carried out. Since statistical fluctuations are large the experimental results have been normalized to the calculated results and only the relative shapes of the two should be compared.

The moderate agreement between the Hauser–Feshbach calculations and experimental results near these energies indicates that potential P3 is bringing in approximately the right angular momentum. However, there is obviously insufficient evidence to make definite spin assignments.

(c) $^{12}\text{C}+^{16}\text{O}$ Elastic Scattering Cross Sections

Coulomb scattering completely dominates the experimental results seen in Figs 4a–4f below 7 MeV, and it heavily masks the results at other energies. The fact that structure can be seen at the most backward angles (154.5° and 149.5°) of similar width to the structure seen in the total reaction cross section suggests that l values 4 and 5 are not present for the resonance at 8.3 MeV. This is a rather surprising result in view of the discussion in subsections (a) and (b) above.

However, calculations using P1 also produce structure at this energy for angles 154.5° and 149.5° . That most of this structure is due to l values 0 and 1 resonating for the second time is demonstrated by comparing these results with those obtained using potential P3. In this case, l values 0 and 1 do not resonate for the second time (see Section 4a and Fig. 6e). Unfortunately, it cannot be stated that this indicates the nonexistence of a repulsive core because of the rather poor overall fit to the elastic scattering results, particularly at the most forward angles (85.7° and 90.0°) where Coulomb scattering dominates. This poor fit is due partly to the second ($l = 0$) resonance in P1 and partly because the resonances are too strong in general. The latter conclusion is consistent with their fits to the Σ factors in Figs 6c and 6f having dips between resonances much lower than the actual measurements. Therefore increasing the imaginary part in P1 and P3 (as in P2 and P4, see Table 2) does lead to slightly better fits but the structure at the most backward angles is then considerably damped. Thus, it is not clear whether the optical potential of equation (5) is appropriate for simultaneously fitting reaction and scattering data.

5. Conclusions

The present work, which reports detailed measurements of elastic scattering in $^{12}\text{C}+^{16}\text{O}$ near the Coulomb barrier, was undertaken to extend the work of Nagorcka and Newton (1972). They showed that a reasonably satisfactory fit may be made to the total reaction cross section induced by $^{12}\text{C}+^{16}\text{O}$ using an optical potential of conventional profile. Though the latter appears reasonably consistent with the shape of $^{12}\text{C}(^{16}\text{O}, \alpha)^{24}\text{Mg}$ angular distributions, it now appears that the conventional optical potential, described by a few parameters, is inadequate to provide a simultaneous fit to all known data. Because of this, we must regard the spin assignments made by Nagorcka and Newton as inconclusive.

The inability to obtain fits with a conventional optical potential may seem surprising, considering the fact that there are actually ambiguities in parameter values found from fits to heavy-ion elastic scattering (Maher *et al.* 1969). Basically, the problem is one of fitting apparent resonances in yield curves whose gross structure is best described by a nonresonant diffraction pattern, particularly for energies above the

barrier (Malmin *et al.* 1972). We assumed, for reasons discussed in Section 4, that the resonances occur in the entrance channel involving ^{12}C and ^{16}O in their ground states, but the constraints are too severe to allow the use of an energy- and angular momentum-independent potential. It is perhaps not surprising that such a simple model fails, and it is of interest here to discuss several more perceptive approaches recently made to the problem.

Following the observation that above-barrier elastic scattering angular distributions show pronounced diffraction structure at both forward and backward angles, Cherdantsev *et al.* (1975) proposed using a two-centre potential derived from the well-known Strutinsky model for fission (Mosel *et al.* 1970; Pruess and Greiner 1970). The excellent fits obtained appear to confirm the effects of strong deformation, with two distinct minima in the effective potential.

A more fundamental approach to the problem has been made by Baye and Reidmeister (1976), based on a microscopic description of single-particle orbitals for the separate ^{12}C and ^{16}O nuclei. This approach includes the effects of antisymmetrization, which does present computational difficulties due to the large number of Slater determinants needed to describe the nonclosed-shell nature of the ^{12}C ground state. However, satisfactory agreement is claimed with known levels in the composite system (including some of the present results). One result of the model is a correct prediction of splitting between rotation bands of odd and even orbital angular momenta. By comparison, our optical potential lacks the essential l dependence and the deformation effects of both the methods described above.

Since the gross-structure effects are dominant in the reactions with such ions as ^{12}C and ^{16}O , it would obviously be important to know the scattering and reaction cross sections of other particles of comparable masses. In line with this, some work has been undertaken (Switkowski *et al.* 1976) to study the reactions of all available pairs of B, C, N and O nuclei. It will obviously be decisive for the new models to be tested with these data. It is interesting to note that these models place, in common with our optical potential approach, an emphasis on the importance of interactions in the entrance channel. The experiments of Switkowski *et al.* should provide direct information on the usefulness of this basic assumption, as well as more particular tests of the effectiveness of the newer models.

References

- Almqvist, E., Bromley, D. A., and Kuehner, J. A. (1960). *Phys. Rev. Lett.* **4**, 515.
 Baye, D., and Reidmeister, G. (1976). *Nucl. Phys. A* **258**, 157.
 Brueckner, K. A., Buchler, J. R., and Kelly, M. M. (1968). *Phys. Rev.* **173**, 944.
 Cherdantsev, P. A., Dhernov, I. P., and Vershinin, G. A. (1975). *Phys. Lett. B* **55**, 137.
 Endt, P. M., and Van der Leun, C. (1967). *Nucl. Phys. A* **105**, 1.
 Fliessbach, T. (1971). *Z. Phys.* **247**, 117.
 Groce, D. E., and Lawrence, G. P. (1965). *Nucl. Phys.* **67**, 277.
 Halbert, M. L., Durham, F. E., Moak, C. D., and Zucker, A. (1967). *Phys. Rev.* **162**, 919.
 Kuehner, J. A., and Almqvist, E. (1964). *Phys. Rev.* **134**, B1229.
 Lane, A. M., and Thomas, R. G. (1958). *Rev. Mod. Phys.* **30**, 257.
 McFadden, L., and Satchler, G. R. (1966). *Nucl. Phys.* **84**, 177.
 Maher, J. V., Sachs, M. W., Siemssen, R. H., and Bromley, D. A. (1969). *Phys. Rev.* **188**, 1665.
 Malmin, R. E., Siemssen, R. H., Sink, D. A., and Singh, P. P. (1972). *Phys. Rev. Lett.* **28**, 1590.
 Mazarakis, M., and Stephens, W. (1972). *Astrophys. J.* **171**, L97.
 Michaud, G. J., and Vogt, E. W. (1972). *Phys. Rev. C* **5**, 350.
 Mosel, V., Thomas, T. D., and Riesenfelt, P. (1970). *Phys. Lett. B* **33**, 565.

- Nagorcka, B. N. (1973). Ph.D. Thesis, Australian National University.
- Nagorcka, B. N., and Newton, J. O. (1972). *Phys. Lett. B* **41**, 34.
- Patterson, J. R., Nagorcka, B. N., Symons, G. D., and Zuk, W. M. (1971). *Nucl. Phys. A* **165**, 545.
- Patterson, J. R., Winkler, H., and Zaidins, C. S. (1969). *Astrophys. J.* **157**, 367.
- Perey, C. M., and Perey, F. G. (1963). *Phys. Rev.* **132**, 755.
- Pruess, K., and Greiner, W. (1970). *Phys. Lett. B* **33**, 197.
- Reidmeister, G. (1972). *Nucl. Phys. A* **197**, 631.
- Rosen, L., Beery, J. G., and Goldfaber, A. S. (1965). *Ann. Phys. (New York)* **34**, 96.
- Scheid, W., and Greiner, W. (1969). *Z. Phys.* **226**, 364.
- Spinka, H., and Winkler, H. (1972). *Astrophys. J.* **174**, 455.
- Switkowski, Z. E., Stokstad, R. G., and Wieland, R. M. (1976). *Nucl. Phys. A* **274**, 202.

Manuscript received 1 April 1976, revised 2 August 1976

